ASTRONAUTICS DIVISION
CHANCE VOUGHT CORP., Dallas, Tex. Astronautics Div.

1796101

Title

THE PREDICTION OF OXIDATION RATES OF CARBONACEOUS MATERIALS FROM PLASMA ARC TESTS

00.241

by

J. K. Haviland and J. E. Medford [1963] 41p refs

Presented at Sixth Biennial Conference on Carbon,
The University of Pittsburgh,
June 17-21, 1963

(Nasa Contract NAS9-576, and Contracts AF 33(616)7947 and AF33(657)8057)

1126

ENCLOSURE (1) TO
CV LETTER NO.
3-50000/32-916

Conf

ABSTRACT

1128

A series of stagnation point plasma arc tests on specimens of carbonaceous material was examined to find out whether the loss of mass could be explained in terms of oxidation of the carbon. Up to a surface temperature of 4000°F, it was found that it could be predicted in terms of the rate of diffusion of oxygen through the boundary layer, computed by Lewis analogy from the known heat flux and driving enthalpy. Best results were obtained by assuming that carbon monoxide was formed, and by using the net heat flux corrected for hot wall and transpiration cooling effects. One series of specimens exhibited marked oxidation resistance, and here the loss rate conformed to the half order Arrhenius equation, in which Lewis analogy was again used to compute the partial pressure of oxygen near the wall. In this case it was possible to compute the reaction rate coefficient of oxidation for the material. Above 4000°F, it was found that additional mass loss was caused by spalling. This was a strong function of temperature, and could be correlated by an equation of the Arrhenius form, although insufficient data was available to determine pressure effects. It is concluded that sufficient information can be obtained from plasma tests to compute the oxidation and spalling rates of a carbonaceous material on a re-entry vehicle.

AUTHOR

ACKNOWLEDGMENT

The original data on which this work was based was obtained under a program funded by the Directorate of Materials and Processes, Aeronautical Systems Division, Air Force Systems Command, Wright Patterson Air Force Base, Ohio, under Contract Nos. AF 33(616)-7947 and AF 33(657)-8057. Additional test data was obtained under a program funded by the Spacecraft Research Division of the Manned Spacecraft Center, National Aeronautics and Space Administration, Houston, Texas under Contract No. NAS 9-576.

SYMBOLS

A = Reduced reactivity, $lb/ft^2\text{-}sec\text{-}atm^{1/2}$

B = Diffusion parameter, dimensionless

C = Spalling constant, $lb/ft^2\text{-}sec$

C_{ox} = Mass fraction of oxygen

c_p = Specific heat of fluid, BTU/lb°R

D = Diffusion coefficient for oxygen, ft^2/sec

$D = K_o e^{-T_{ox}/T_w}$, dimensionless

E = Activation energy of oxidation, K cal/mole

h_{EFF} = Effective skin coefficient, $LB/ft^2\text{-}sec°R$

i = Enthalpy of fluid, BTU/lb

K_o = Dimensionless reaction rate coefficient

K_s = Dimensionless spalling coefficient

k = Conductivity of fluid, BTU/ft-sec°R

k_{ox} = Reaction rate coefficient of oxidation, $lb/ft^2\text{-}sec\text{-}atm^{1/2}$

L = Lewis number = $\rho D c_p / k$

L_{EFF} = Effective Lewis number

$\dot{M}$ = Mass loss rate, $lb/ft^2\text{-}sec$

$\dot{M}_E$ = Rate of loss due to oxidation, $lb/ft^2\text{-}sec$

$\dot{M}_{ox}$ = Rate of diffusion of oxygen, $lb/ft^2\text{-}sec$

$\dot{M}_{sp}$ = Rate of loss due to spalling, $lb/ft^2\text{-}sec$

$\dot{M}_{TOT}$ = Total rate of loss, $lb/ft^2\text{-}sec$

P_{ox} = Quantity used in determining oxidation constants

P_{SPALL} = Quantity used in determining spalling constants

p = Local static pressure, atmospheres

p_{o_2} = Partial pressure of molecular oxygen, atmospheres

q = Heat flux, BTU/ft^2-sec

q_{BLOW} = Convective heat flux with transpiration cooling, BTU/ft^2-sec

R = Universal gas constant, K cal/mole°R

R_c = Fraction of carbon in material

R_{ox} = Ratio of oxygen to material oxidized

T_{ox} = Activation temperature of oxidation, °R

T_s = Spalling temperature, °R

T_w = Temperature at surface, °R

X = Dimensionless oxidation rate

Y = Dimensionless mass loss rate or oxidation parameter

δ = Boundary layer thickness, ft

K = Transpiration coefficient, dimensionless

Subscripts

COLD - Cold wall conditions

HOT - Hot wall conditions

INIT - Initial trial value

e - Conditions outside boundary layer

R - Recovery conditions

w - Surface conditions

α - Species of ablating material

1.0 INTRODUCTION

In the search for high temperature materials to withstand re-entry conditions, a considerable amount of attention has been given to the possible use of graphite and other carbonaceous materials. Because of its high temperature of sublimation, its superior strength to weight ratio, and its high emissivity, it would be an ideal material for a reradiating heat shield, but for one problem, that it oxidizes at a relatively rapid rate. Anti-oxidation coatings have been developed for graphite, but suitable coatings are generally restricted to temperatures of about 3200°F, little better than can be obtained with coated refractory metals. In principle, it would seem possible to coat graphite with a high temperature ceramic, such as zirconia or thoria, but such materials are too brittle for use as coatings. For these reasons, the oxidation of carbonaceous materials has been studied, and a number of tests have been made in a plasma arc facility to verify theoretical predictions, and to obtain fundamental properties.

It is generally agreed that the oxidation of carbonaceous materials can be divided into three regimes, depending upon the processes which determine the rate of oxidation. These are:

(1) The reaction rate control regime in which the oxidation rate is controlled by surface kinetics processes, including absorption of reactants on the surface, chemical reaction on the surface and desorption of products from the surface[1].

(2) The diffusion control regime in which the oxidation rate is controlled by diffusion of reactants to the surface or diffusion of products from the surface[1].

(3) The transition regime in which both diffusion and surface kinetics determine the oxidation rate.

The reaction rate control regime has been studied extensively, both theoretically and experimentally. Glasstone, et al[1] present relations derived from absolute reaction rate theory which give the reaction rate for a true surface reaction applicable to non-porous materials. Wheeler[2] has developed a model for the reaction of a gas in the pores of a solid which is applicable to a porous material. Blyholder and Eyring[3&4] further developed and obtained experimental confirmation for Wheeler's model.

TU, Davis, and Hottel[5] in 1934 and more recently, Moore and Zlotnick[6] have studied the transition regime. Moore and Zlotnick were quite sophisticated in their treatement of the boundary layer and surface kinetics, however, their study lacked the benefit of experimental confirmation. Bradshaw[7] has studied the transition regime experimentally, but it is not known whether his results in this regime have been compared to theory, quantitatively.

The diffusion control regime has received extensive theoretical study[8-12]. However, here again, there appears to be a lack of theoretical studies which have been confirmed by experimental data.

This paper is a study of all three oxidation regimes, and, in addition, of mass loss by spalling. Both theoretical and experimental techniques have been employed to establish techniques for the investigation of mass loss of carbonaceous materials in a gas stream. The methods developed should also prove invaluable for the investigation of carbonaceous materials incorporating additives, internally diffused coatings, etc., for the reduction of oxidation rates. They are not essentially limited to carbonaceous materials, although other materials have not been tested to date.

1.1 Summary

A proprietary method of forming reinforced carbonaceous materials of high strength and porosity was developed by Chance Vought Corp. A large number of plasma tests have been run on specimens of this material in the 180 KW plasma arc facility of the Ling-Temco-Vought Research Center. The cold wall heating rates for these tests ranged from 8 to 730 BTU/ft^2-sec, as determined by calorimeters, the air enthalpies ranged from 3500 to 16,000 BTU/lb as determined by energy balance and sonic throat methods, and the surface temperatures ranged from 1650° F to 5600° F as determined by optical pyrometers with suitable corrections. These conditions are typical of those experienced by manned re-entry vehicles. A large number of these plasma arc tests were carried out by Carlson, et al[13]. In analyzing these results, it was noted that the surface recessions could be approximately correlated on the assumption that the rate of diffusion of oxygen to the surface could be predicted by what might be termed 'Lewis analogy'. A typical material studied was designated Matrix II. Several of the materials were intended to resist oxidation, and one appeared particularly successful. This was designated as Matrix III.

It was decided that the Lewis analogy might be used in predicting surface recession rates in IBM studies of ablators. To obtain correct predictions of surface recession at low temperatures, the oxidation reaction suggested by Nolan and Scala[14] was used in conjunction with the diffusion equation.

In order to verify the equations, the test results of Carlson, et al[13], were reanalyzed. At the same time, equations were developed to predict the rate of mechanical erosion, or 'spalling', which was seen to occur at high temperatures, and methods were developed to obtain the material constants from test data. The results obtained for Matrices II and III are given in Section 3 of this paper.

A heat shield system is currently under development, in which a reinforced carbonaceous face is used (F. C. Smith[15, 16]). The results of a series of oxidation tests on this material are also given in Section 3.

1.2 Conclusions

1. A set of equations has been derived to account for surface recession rates due to oxidation and spalling, and a method has been developed to derive the required material constants from plasma arc test results. Using this approach, it has been shown that test results can be correlated to within experimental scatter. This report has been restricted to demonstrating the feasibility of the approach, and insufficient test data has been available to permit the application of statistical methods in obtaining correlation.

2. Materials tested to date are restricted to a particular formulation, referred to as reinforced carbonaceous material. It is believed, however, that the methods developed here are applicable to any material which undergoes oxidation, and in which the chemical form is relatively independent of temperature.

3. One particular material, referred to as Matrix III, showed particular promise as an oxidation resistant material. This relies on an internally diffused coating, as opposed to a surface coating, and is therefore not liable to suffer catastrophic failure.

4. Due to limitations imposed by the performance of the plasma arc, the effects of pressure could not be determined.

2. THEORY OF OXIDATION

There are three basic mechanisms by which the surface can recede on a material composed mainly of carbon or graphite, when exposed to a stream of high temperature air.

(1) Oxidation: This is further divided up into three regimes:

(a) The reaction controlled regime, at low temperatures, in which the air at the surface is oxygen rich, and oxidation is controlled by the chemical reaction rate.

(b) The transition regime, at intermediate temperatures, in which the rate of oxidation is sufficiently high to reduce the concentration of oxygen near the surface.

(c) The diffusion controlled regime, at high temperatures, in which the oxidation rate is controlled by the available supply of oxygen diffusing through the boundary layer to the surface.

(2) Spalling: This covers a multitude of poorly defined mechanisms by which material is removed from the surface in excess to that removed by oxidation. Spalling typically occurs at high temperatures, and is probably dependent on shear forces or total pressure.

(3) Sublimation: This is the fundamental ablation process, in which the material is converted to gas, and absorbs heat of vaporization in the process. The process of sublimation may be completely masked by spalling, so that it cannot be detected independently. Since sublimation of the surface of a heat shield is well understood, and since the temperatures considered in this study are below the sublimation temperature of carbon, it will not be considered here.

2.1 Derivation of Oxidation Equations

The rate of mass loss due to oxidation by molecular oxygen is given by the equation,

$$\dot{M}_E = k_{ox} (\rho_{o_2})_w^{1/2} e^{-T_{ox}/T_w} \qquad 2.1.1$$

where $\dot{M}_E$ is the effective mass loss per unit area due to oxidation, including material which does not oxidize, but is released in the oxidation process; k_{ox} is the reaction rate coefficient, sometimes referred to as the "specific reactivity"; $(\rho_{o_2})_w$ is the partial pressure of molecular oxygen at the surface; T_{ox} is the activation temperature, equal to E/R, where E is the activation energy; and T_w is the surface temperature. There is still some disagreement as to the precise form of this equation, which has been taken from Nolan and Scala (Reference 14). In particular, it is not certain that the index (order of reaction) should be 1/2. Blyholder and Eyring indicate that from 1510 to 1870° R for porous graphite the index is indeed 1/2. But for higher temperatures and/or non-porous graphite, they found values from zero to 3/4 [3,4]. Furthermore, the specific reactivity is believed to be temperature dependent,[1,3,4]. However, Blyholder and Eyring indicate that for porous graphite the reactivity is proportional to temperature to the 1/4 power and that for non-porous graphite, the power is unity,[3,4]. Thus, the temperature dependence of K_{ox} is quite weak compared to the exponential term in Equation 1. Finally, the aforementioned authors found that above 1870° F for porous graphite T_{ox} changes.[4]

If atomic oxygen is present at the surface, a second term should be added to Eqn. 1. It has been assumed here that all oxygen reaching the surface is recombined.

The relationship between the rate of diffusion of oxygen and the rate of heat conduction through the boundary layer can be derived in terms of an effective Lewis number. We assume that the boundary layer thicknesses for heat conduction and diffusion are equal, and given by δ. Then the heat transfer rate in the presence of transpiration cooling from the gaseous products of ablation, q_{BLOW} is (see also Section 2.3).

$$q_{BLOW} = \left([\overline{k/c_p}]\, 1/\delta - \Sigma(\alpha)\, \dot{M}_\alpha K_\alpha \right)(i_R - i_w)$$
$$= h_{EFF}\,(i_R - i_w) \qquad 2.1.2$$

where $\overline{[k/c_p]}$ is a suitably averaged ratio of conductivity k divided by specific heat c_p in the boundary layer; $\dot{M}_\alpha$ and K_α are rates of injection and transpiration coefficients, respectively, for a given species α in the gaseous products of ablation; i_R and i_w are the values of the enthalpy of the air at recovery and wall temperatures, respectively; and h_{EFF} is the effective skin coefficient.

The rate of diffusion of oxygen, $\dot{M}_{ox}$ per unit area, is given by;

$$\dot{M}_{ox} = \overline{\rho D}\,(c_{ox_e} - c_{ox_w})/\delta \qquad 2.1.3$$

where $\overline{\rho D}$ is a suitably averaged product of density ρ, and diffusion coefficient D, in the boundary layer; and c_{ox_e}, c_{ox_w} are mass concentration ratios of oxygen at the outer surface of the boundary layer, and at the wall, respectively.

Noting that the Lewis number is defined by;

$$L = \rho D c_p/k \qquad 2.1.4$$

we can define an effective Lewis number, L_{EFF}, by;

$$L_{EFF} = \frac{\overline{\rho D}}{(\overline{[k/c_p]} - \delta \Sigma(\alpha)\dot{M}_\alpha K_\alpha}$$

$$= \frac{\dot{M}_{ox}}{h_{EFF}\,(c_{ox_e} - c_{ox_w})} \qquad 2.1.5$$

after substituting from Eqns. 2 & 3.

The effective Lewis number includes the effects of transpiration cooling, which is assumed to block heat conduction and oxygen diffusion through the boundary layer in equal ratios. Since the Lewis number normally has a value close to unity, it may be assumed that L_{EFF} is also close to unity.

At sufficiently low temperatures, the oxygen reaching the surface is mainly molecular, and the partial pressure of oxygen near the wall is;

$$(p_{O_2})_w = p\,c_{ox_w}\,(M.W._{(AIR)}/M.W._{(O_2)}) \qquad 2.1.6$$

where p is the local static pressure; and $M.W._{(AIR)}$, $M.W._{(O_2)}$ are molecular weights of air and O_2 respectively.

The ratio of oxygen consumed at the surface to the effective mass loss due to oxidation can be expressed as the constant ratio;

$$R_{ox} = \dot{M}_{ox} / \dot{M}_E \qquad 2.1.7$$

if one chemical reaction is assumed to take place, for example, if the reaction is*;

$$2C + O_2 + \text{Non-oxidizing material} \longrightarrow 2CO + \text{Non-oxidizing material} \qquad 2.1.8$$

and if R_c is the proportion of carbon in the total material;

$$R_{ox} = \left(A.W._{(ox)} / A.W._{(C)}\right) R_c = \frac{4}{3} R_c \qquad 2.1.9$$

where $A.W._{(ox)}$ and $A.W._{(C)}$ are atomic weights of oxygen and carbon, with values of 16 and 12 respectively.

Substituting the value of $(p_{O_2})_w$ from Eqn. 2.1.6 into 2.1.1, and eliminating c_{ox_w} and $\dot{M}_{ox}$ from Eqns. 5 and 7 respectively.

$$\dot{M}_E = A \rho^{1/2} \left(1 - B \dot{M}_E / h_{EFF}\right)^{1/2} e^{-T_{ox}/T_w} \qquad 2.1.10$$

where $$A = k_{ox} \left\{ \left(M.W._{(AIR)} / M.W._{(O_2)}\right) c_{oxe} \right\}^{1/2} \qquad 2.1.11$$

$$B = R_{ox} / L_{EFF}\, c_{oxe} \qquad 2.1.12$$

Equation 2.1.10 gives the oxidation rate of carbon or graphite by molecular oxygen in the reaction rate control, transition, and diffusion rate control regimes. The terms A, B and T_{ox} depend on the material and on the nature of the atmosphere. They are approximately constant for any given re-entry, provided that chemical reactions do not take place in the material which change the value of k_{ox}. The terms ρ, h_{EFF}, and T_w define the environment at the surface, and vary during re-entry.

Additional material is lost by spalling and by sublimation. It is assumed that these can be characterized by an equation of the form;

$$\dot{M}_{SP} = C(\rho)\, e^{-T_s/T_w} \qquad 2.1.13$$

where $C(\rho)$ is a coefficient, dependent to an unknown extent on aerodynamic forces and other variables, and T_s is a characteristic spalling temperature, equivalent to the activation temperature T_{ox} in Eqn. 2.1.1.

The total mass loss rate now becomes;

$$\dot{M}_{TOT} = \dot{M}_E + \dot{M}_{SP} \qquad 2.1.14$$

* Blyholder and Eyring [3,4] indicate that CO is the primary product of graphite oxidation from 1510° R to 2230° R and probably to 2770° R.

2.2 Dimensionless Form of Equations

Equations 2.1.10 and 11 can be put into dimensionless form by taking

$X = B\dot{M}_E / h_{EFF}$ = dimensionless oxidation rate

$Y = B\dot{M}_{TOT} / h_{EFF}$ = dimensionless mass loss rate or oxidation parameter

and writing them in the form

$$X = K_o (1 - X)^{1/2} e^{-T_{ox}/T_w} \qquad 2.2.1$$

$$Y = X + K_s e^{-T_s/T_w} \qquad 2.2.2$$

where $K_o = AB\rho^{1/2} / h_{EFF}$ = dimensionless reactivity

$K_s = BC / h_{EFF}$ = dimensionless spalling constant

The solution of Eqn. 1 is

$$X = \tfrac{1}{2} D \left\{ \sqrt{D^2 + 4} - D \right\} \qquad 2.2.3$$

where $D = K_o e^{-T_{ox}/T_w}$

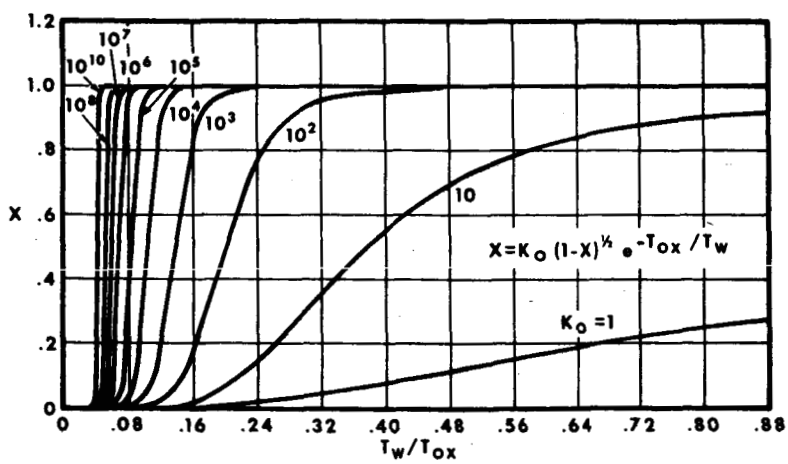

FIGURE 1 DIMENSIONLESS OXIDATION RATE (X) VS. TEMPERATURE RATIO T_W/T_{OX} FOR VARIOUS VALUES OF DIMENSIONLESS REACTION RATE K_O

The dimensionless oxidation rate X is plotted in Figure 1 as a function of T_w/T_{ox} for a number of values of the dimensionless reactivity K_o. It is seen that at low temperatures the oxidation rate increases with temperature as governed by reaction kinetics, but as the temperature increases further, it undergoes transition to a constant rate determined by oxygen diffusion. Decreasing the reactivity has the effect of raising the temperature at which transition occurs and of broadening the transition temperature regime. Furthermore, the extent to which decreasing the reactivity of a given type of material (by use of oxidation inhibitors for example) will decrease the oxidation rate depends strongly upon the temperature range of interest. It will be shown in Section 3 that the dimensionless form of the oxidation relations is extremely useful in evaluating experimental results.

2.3 Computation of Effective Skin Coefficient

Before plasma arc test results can be reduced, the effective skin coefficient h_{EFF} must be determined, as defined in Eqn. 2.1.2. Several methods are available for determining recovery enthalpy in the plasma stream, i_R, and the enthalpy at wall conditions, i_w can be determined from a Mollier diagram, if local pressure and surface temperature are known. The heat flux, however, is measured by a calorimeter having the same shape as the test specimen, and must be corrected for the effects of wall temperature and transpiration cooling.

The corrected convective heat flux can be written in the approximate form

$$q_{BLOW} = q_{HOT} - \Sigma(\alpha)\,\dot{m}_\alpha K_\alpha (i_R - i_w) \qquad 2.3.1$$

where $\dot{m}_\alpha$, K_α, i_R, and i_w, have already been defined in Eqn. 2.1.2, and q_{HOT} is the convective heating to the hot wall, which can be expressed in the form

$$q_{HOT} = q_{COLD}\left(\frac{i_R - i_w}{i_R - i_{COLD}}\right) \qquad 2.3.2$$

Here, q_{COLD} is the equivalent heat flux to a cold wall, as measured by a calorimeter, where the enthalpy of the air at cold wall conditions is i_{COLD}.

2.4 Comparison with Method of Nolan and Scala

Nolan and Scala[14] use a somewhat different method for computing the oxidation rate, in which rates of oxidation in the reaction and diffusion regimes are first calculated, and then combined so that the result is asymptotically correct. Their approach can be summarized as follows:

The mass loss rate in the reaction controlled regime is given by Eqn. 2.1.1 in the form

$$\dot{m}_{REACT} = k_{ox}(p_{O_2})_e^{1/2} e^{-T_{ox}/T_w} \qquad 2.4.1$$

The skin coefficient is computed from the equation

$$h_{EFF} = \frac{q_{HOT}}{i_R - i_w} = 0.0333\frac{\rho^{1/2} f(\Lambda)}{\sqrt{2R_B}}\left[\frac{\sqrt{2}}{f(\Lambda)}\right]^{\delta} + \text{TERM} \qquad 2.4.2$$

where $f(\Lambda)$ is a function of sweep angle, R_B is an effective nose radius, δ is an index depending on geometry, and 'TERM' is a quantity which is small at high heating rates, and will be ignored in the following analysis. The mass loss rate in the diffusion controlled regime for a carbon or graphite material is given by

$$\dot{m}_{DIFF} = 6.2 \times 10^{-3}\frac{\rho^{1/2} f(\Lambda)}{\sqrt{2R_B}}\left[\frac{\sqrt{2}}{f(\Lambda)}\right]^{\delta} \qquad 2.4.3$$

Referring to Eqn. 2.1.10, it will be noted that the mass loss rate in the diffusion controlled regime can be obtained by equating the term in the brackets to zero, and solving for $\dot{M}_E$. If we then obtain h_{EFF} and $\dot{M}_{DIFF}$ from Eqns. 2 and 3, with TERM = 0, we obtain

$$B = h_{EFF} / \dot{M}_{DIFF} = .0333 / 6.2 \times 10^{-3} = 5.37 \qquad 2.4.4$$

This value is less than the 5.80 reported in Table II for carbon or graphite, as obtained from Eqn. 2.1.12. The mass loss rate in the transition regime is now approximated by

$$\dot{M}_E = \frac{1}{1/\dot{M}_{REACT} + 1/\dot{M}_{DIFF}} \qquad 2.4.5$$

If we multiply this expression through by B/h_{EFF} , and substitute from Eqn. 4, noting that

$$\frac{B\dot{M}_{REACT}}{h_{EFF}} = D \qquad 2.4.6$$

where D is defined in Eqn. 2.2.3, we have

$$X = \frac{1}{1/D + 1} \qquad 2.4.7$$

This expression for D is compared with the expression derived in this report, as given by Eqn. 2.2.3, in Figure 2. It will be noted that the difference is not large.

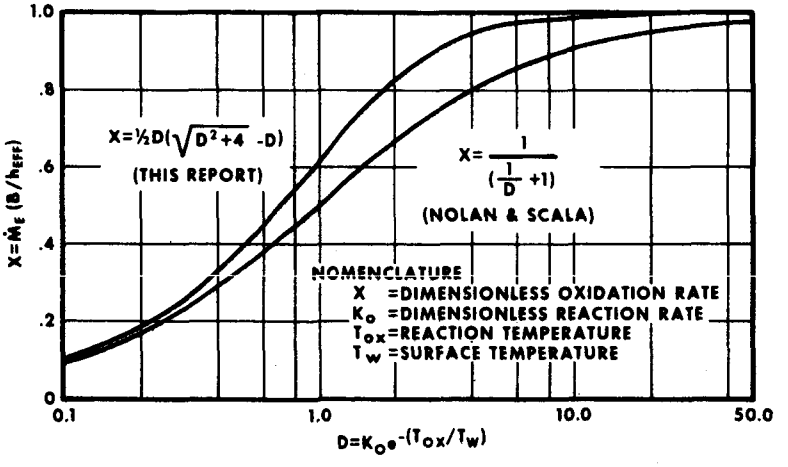

FIGURE 2 COMPARISON OF TWO EXPRESSIONS FOR THE DIMENSIONLESS OXIDATION RATE

3. EXPERIMENTAL RESULTS

3.1 Determination of Oxidation Parameters from Plasma Tests

A large number of plasma tests have been run on specimens of reinforced carbonaceous material, or RCM, in the 180 kW plasma arc facility

of the Ling-Temco-Vought Research Center. The material referred to here is a proprietary system developed by Chance Vought Corp. It is described fully by Carlson, et al[13], and consists of laminated sheets of carbon, or graphite cloth, bonded by a polymer, and then reduced to a char in an oven. The final result is a laminate bonded by long carbon molecules, possessing unusually good structural properties at high temperatures. Although the RCM is mainly carbon, its unique structure derives from its organic origin. Since the material is porous, it can be treated in a number of ways, including the vapor deposition of materials which improve its resistance to oxidation uniformly throughout its thickness. It can also be soaked in a 'filler' material, which ablates when heat is applied, thereby improving its effective insulative properties for limited periods. The RCM may also be graphitized, which modifies its structure somewhat.

Three materials were selected for a detailed study of their oxidation properties, and further information is given on their composition in Table 1. A total of 81 tests is included in this study, and results are detailed in the Appendix.

TABLE I

Composition of Reinforced Carbonaceous Materials

Designation	Matrix II	Matrix III	Face Material
References	13	13	15, 16
Laminate	Graphite	Graphite	Graphite
Graphitized	No	Yes	No
Vapor Deposit	None	Silicon & Zirconium	None
Ablative Fillers	None Polystyrene Nylon 6 Fluoroalkyl Acrylate Ammonium Chloride Borox	None Nylon 6 Ammonium Chloride	None

The first two materials, Matrix II and Matrix III, were tested to determine their performance as ablators, as reported in Reference 13. Test specimens were cylindrical, 3/4 inches in diameter and 1/2 inches long, except for some specimens one inch long, and were tested under stagnation point conditions. The third material, referred to as face material, has been developed as a protective face for a special heat shield system; it

was tested under stagnation point conditions and also under side heating conditions, as reported in Reference 16. Configurations of these test specimens are shown in Figure 3.

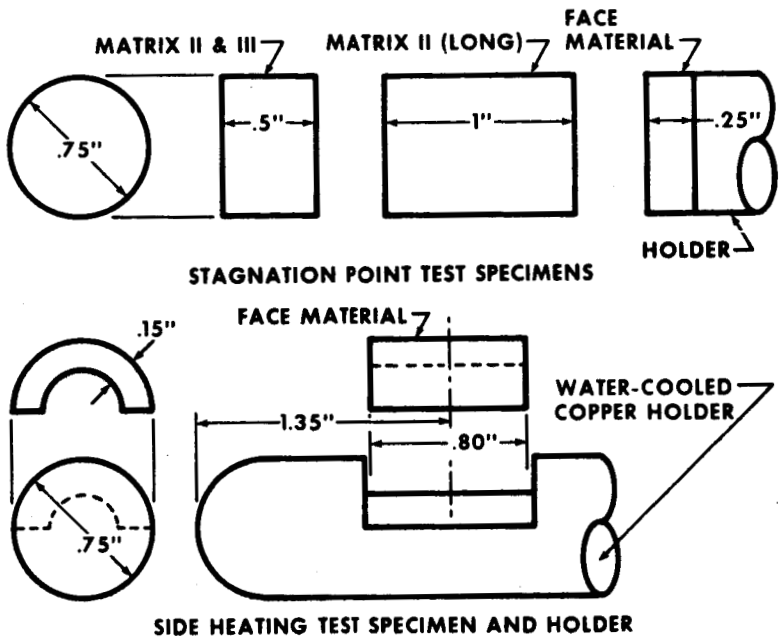

FIGURE 3 PLASMA ARC TEST SPECIMENS

3.2 Determination of Oxidation Parameters

The results of the plasma tests are given in the Appendix. Experimental values of the oxidation parameter Y are shown plotted in Figures 4, 5 and 6 for the material systems. In compiling the values of Y, it was necessary to assume a value for the effective Lewis number, $(L_{EFF})_{INIT}$ so that Y is defined by

$$Y = \frac{B\dot{M}_{TOT}}{h_{EFF}} = \left(\frac{R_{OX}\dot{M}_{TOT}}{h_{EFF}C_{OXe}}\right)\frac{1}{(L_{EFF})_{INIT}} \qquad 3.2.1$$

For any test point lying in the diffusion regime, and below the spalling regime, we should have

$$R_{OX}\dot{M}_{TOT} \approx R_{OX}\dot{M}_E = \dot{M}_{OX}$$

and

$$C_{OXW} \approx 0$$

Thus, from the definition of L_{EFF} given by Eqn. 2.1.5

$$Y = L_{EFF}/(L_{EFF})_{INIT} \qquad 3.2.2$$

For the computations in the Appendix, and the experimental points plotted in Figures 4, 5 and 6, it was assumed that $(L_{EFF})_{INIT} = 1$. Thus, if a distinct diffusion regime exists, the values of Y for any experimental

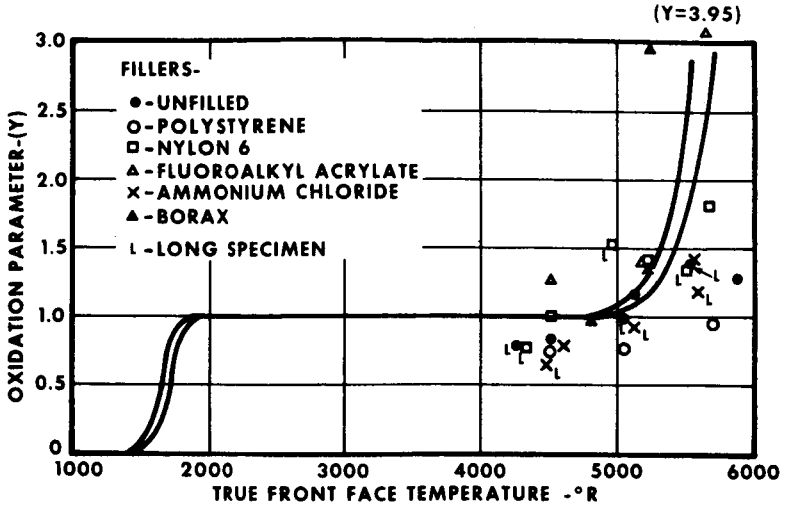

FIGURE 4 EXPERIMENTAL VS. THEORETICAL VALUES OF OXIDATION PARAMETER (Y) MATRIX II

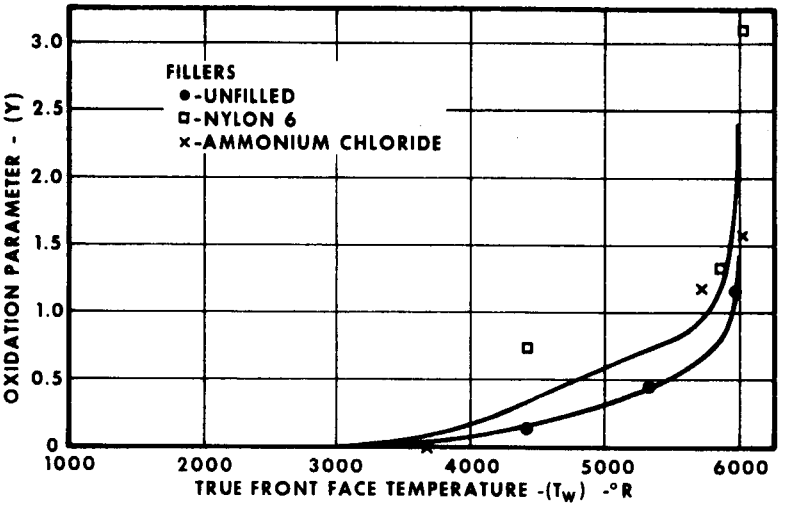

FIGURE 5 EXPERIMENTAL VS. THEORETICAL VALUES OF OXIDATION PARAMETER (Y) MATRIX III

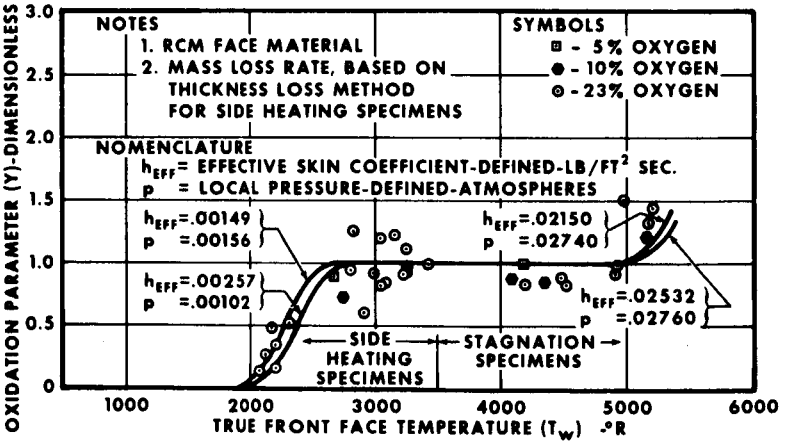

FIGURE 6 OXIDATION PARAMETER VS. SURFACE TEMPERATURE SIDE HEATING AND STAGNATION OXIDATION

points in this regime are equal to the experimental values of L_{EFF}. According to the theoretical curves shown in the figures (the derivation of these curves is explained later), distinct diffusion controlled regimes exist for Matrix II and face material. This regime is characterized by values of Y near unity and invarient with temperature. The number of experimental points for Matrix II, as shown in Figure 4, is insufficient to obtain a good value for L_{EFF} differing significantly from unity, although experimental points lie between 0.75 and 1.0. The experimental points for the face material, as shown in Figure 6, cover the complete diffusion control regime, and values for L_{EFF} lie between 0.8 and 1.25.

For lack of more precise information, it has been assumed that $L_{EFF} = 1.0$. From kinetic theory estimates[17] the Lewis number is of the order of one. Since the rate of loss of carbonaceous material, without oxidation protection, is very nearly proportional to L_{EFF} during re-entry trajectory, a better definition of

L_{EFF} is evidently required. It may be noted that the results of Nolan and Scala[14] indicate that B = 5.37 for carbon and graphite (see Eqn. 2.4.4), whereas B = 5.8 when L_{EFF} = 1 (see Table II). Thus Nolan and Scala's analytical results indicate a value for L_{EFF} of 5.8/5.37 = 1.08, when applied to a typical nose cone, in comparison with the experimental range of 0.75 to 1.25 obtained in plasma tests. In an earlier paper[9] Scala assumed L_{EFF} =1.2. Most other investigators[8, 10, 12] have assumed L_{EFF} = 1.0.

Experimental values for L_{EFF} presented here reflect the assumption that transpiration affects diffusion as well as convective heat transfer through the boundary layer. For specimens without filler, the transpiration cooling reduced the heat flux by less than 11% in all cases, and had it been ignored, experimental values of L_{EFF} would have been reduced by the same percentages. However, for specimens with ablative filler, reductions lay between 16% and 49%, which would have brought the corresponding experimental points well below those for the unfilled specimens. Although the evidence is not conclusive, it does appear necessary to consider transpiration effects when computing oxidation rates in the presence of ablation. When there is no ablation, it does not have much effect on the results, whether or not it is correct.

The experimental results presented in the Appendix have been used to determine values of the oxidation and spalling constants, by methods explained in the following two sections. The results are given in Table II, and have been used to compute the theoretical curves in Figures 4, 5 and 6. Because of the range of values of p and h_{EFF} during the tests, two theoretical curves are shown in each figure, representing the range of experimental conditions. These are summarized in Table III. For comparison, values of the oxidation constants are included in Table II for commercial and pyrolytic graphite, as given by Nolan and Scala[14, 18] and Horton[19].

The test results for Matrix II, as shown in Figure 4, lie mainly in the spalling regime characterized by values of γ considerably greater than unity, and show considerable scatter about the theoretical curve. More regularity can be discerned in the test points for any given material (matrix-filler composite), indicating that the filler material may have an effect on spalling.

The test results for Matrix III, as shown in Figure 4, indicate considerably better agreement with the theoretical curves. In fact, the only bad point is one with nylon filler. The writers have viewed motion pictures of a plasma test on material incorporating nylon, and it was evident that the nylon extrudes from the surface in plastic form. It is possible that this is responsible for mechanical erosion of the surface, causing an excessive mass loss. The significant point about the tests on the Matrix III material was that it exhibited considerable resistance to oxidation. This is evidenced by values of γ in the reaction rate and transition control regimes (γ considerably less than unity) up to extremely high temperatures. In fact the mass loss rate did not exceed the theoretical diffusion controlled rate (γ = 1.0) until a surface temperature of 5750° R was reached, where spalling began to occur.

TABLE II

SUMMARY OF PROPERTIES

MATERIAL	MATRIX II	MATRIX III	FACE	COMMERCIAL GRAPHITE	PYROLYTIC GRAPHITE	PYROLYTIC GRAPHITE (ALTERNATE)	PYROLYTIC GRAPHITE (ALTERNATE)
References				14, 18	14, 18	14, 19	14
Density, lb/ft^3	62.4	62.4	62.4	108	138	138	138
Rc	1.0	.865-.925	1.0	1.0	1.0	1.0	1.0
Act. Energy, K cal/mole	(1)44	36.6	44	44	44	32.8	47.5
T_{ox}, °R	(1)39,800	32,400	39,800	39,800	39,800	29,700	43,000
k_{ox}, $lb/ft^2 sec\ atm^{1/2}$	(1)6.73×10^8	20.2	3.76×10^5	6.73×10^8	4.47×10^4	3.07×10^4	1.28×10^4
(2)A, $lb/ft^2 sec.atm^{1/2}$	3.08×10^8	9.23	1.72×10^5	3.08×10^8	2.05×10^4	1.41×10^4	0.59×10^4
(2)B	5.8	5.03-5.36	5.8				
T_s, °R	157,500	346,600	(3)157,500				
Mean P for spalling, atm	.07	.07					
C, $lb/ft^2 sec$	1.36×10^{10}	6.86×10^{22}	(3)1.36×10^{10}				

- Assumed the same as commercial graphite
- Values for 23% oxygen
- Assumed same as Matrix II

TABLE III

CONSTANTS FOR THEORETICAL OXIDATION PARAMETERS
(23% Oxygen)

MATERIAL		MATRIX II	MATRIX III	FACE
T_{ox}, °R		39,800	32,400	39,800
A, $lb/ft^2 \cdot sec \cdot atm^{1/2}$		3.08×10^8	9.23	1.72×10^5
B		5.8	5.22	5.8
T_s, °R		157,500	346,500	157,500
C, $lb/ft^2 \cdot sec$		1.36×10^{10}	6.88×10^{22}	1.36×10^{10}
Transition Regime:				
p, atmospheres,	Max	0.065	0.065	.00156
	Min	0.05	0.05	.00102
h_{EFF}, $lb/ft^2 \cdot sec$	Max	0.04	0.04	.002570
	Min	0.02	0.02	.001491
K_o	Max	2.28×10^{10}	615	2.63×10^7
	Min	10^{10}	270	1.245×10^7
Spalling Regime:				
p, atmospheres,	Max	0.065	0.065	.02760
	Min	0.05	0.05	.02740
h_{EFF}, $lb/ft^2 \cdot sec$.	Max	0.04	0.04	.02532
	Min	0.02	0.02	.02150
K_s	Max	3.95×10^{12}	18×10^{24}	3.66×10^{12}
	Min	1.97×10^{12}	9×10^{24}	3.11×10^{12}

The plasma arc tests reported on Matrices II and III were originally carried out to determine the effectiveness of RCM as an ablative material. Although the test results were used in developing the theory presented here, the presence of fillers introduced added complications. The tests on the face material were carried out specifically to determine its oxidation properties, and both side heating and stagnation point tests were made to increase the range of surface temperatures. The results shown in Figure 6 cover tests in 5, 10 and 23% oxygen, mixed with nitrogen, and fall into the transition, diffusion, and spalling regimes. Scatter of the test points about the theoretical curves is highest for the side heating specimens in the transition regime, but this may be due to experimental difficulties. Mass losses had to be kept small because the specimens were only 0.15 inches thick, and erosion rates varied considerably over the surfaces, due to flow effects. The mass losses actually given were computed from recessions measured at the same locations as the calorimeters used in determining the cold wall heat fluxes. Mass losses at the stagnation point were obtained by weighing, however, mass losses were also computed from the measured recession of the face material specimen (in brackets in the Appendix) to determine whether oxidation occurred in depth. Comparison of the two sets of figures indicates that this is not the case.

Points corresponding to 0% oxygen could not be included in this plot. Therefore, the mass loss rates, $\dot{M}_{TOT}$, are shown in Figure 7 for all tests on the face material. Three of the stagnation point specimens in 0% oxygen showed considerable mass losses at around 3,500°R, while the side heating specimens at lower temperatures showed no mass loss. Since the losses occurred well below the spalling regime as evidenced by the results in Figure 6, no reasonable explanation can be given.

Due to the severe restrictions on the range of pressures obtainable in the plasma arc, it was not possible to check the dependency of oxidation and spalling on pressure. Other methods are available to verify the half order of reaction assumed in Eqn. 2.1.1, but the determination of the pressure dependency of the spalling coefficient (C in Eqn. 2.1.13) will present a serious problem.

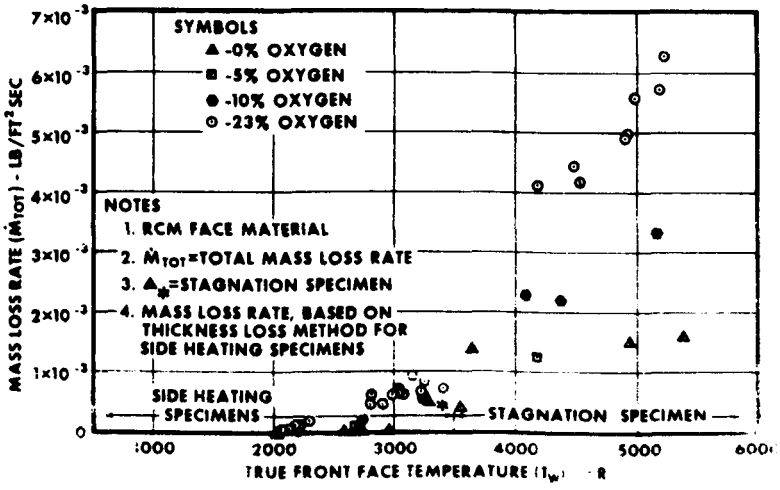

FIGURE 7 MASS LOSS RATE VS. SURFACE TEMPERATURE SIDE HEATING AND STAGNATION OXIDATION

3.3 Determination of Oxidation Constants

Experimental values of the oxidation parameter Y obtained in the transition regime, and at temperatures for which spalling is negligible, can be used to determine the oxidation constants. In the temperature range defined, we have $Y = X < 1$, and can rewrite Eqn. 2.2.1 in the form

$$P_{ox} = \frac{Y^2}{1-Y} \frac{h_{EFF}}{p} = (AB)^2 e^{-2T_{ox}/T_w} \qquad 3.3.1$$

Taking logarithms of both sides

$$\ln P_{ox} = \ln (AB)^2 - 2\, T_{ox}/T_w \qquad 3.3.2$$

Thus if experimental values of P_{ox} are plotted against $1/T_w$ on semilog paper, the slope of the best fit line is equal to $-2\, T_{ox} \log_{10} e$ and the intercept is equal to $\log_{10} (AB)^2$. A plot of this type is shown in Figure 8 for Matrix III material, and includes all test points below 5500°R. Another plot is shown in Figure 9 for the face material, and includes six side heating test points below 2300°R. The test point for nylon filler is questionable, as explained in Section 3.2. All of these tests were made in 23% oxygen. The values of P_{ox} shown in the two figures were obtained from the Appendix.

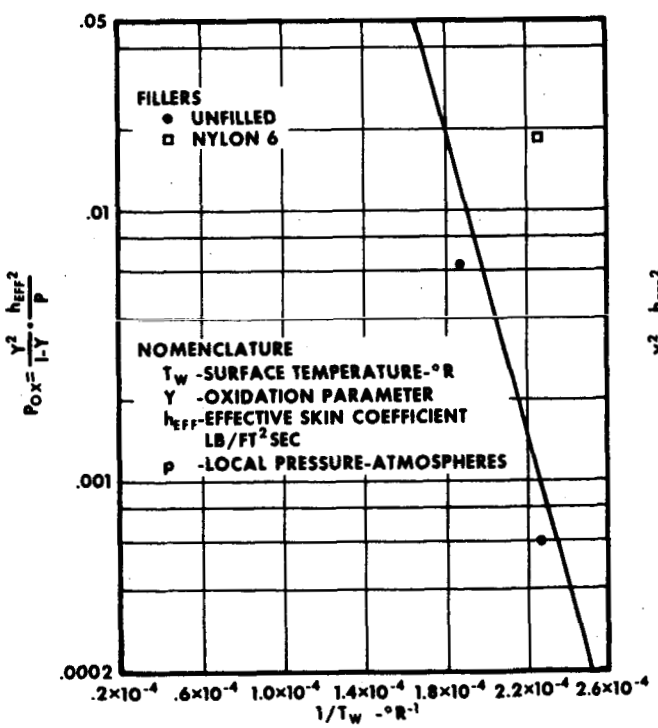

FIGURE 8 GRAPHICAL DETERMINATION OF OXIDATION CONSTANTS MATRIX III

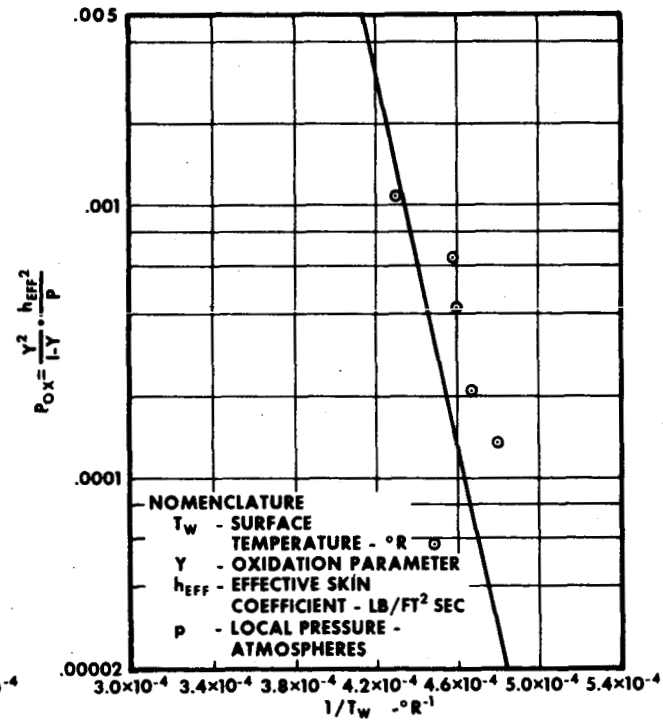

FIGURE 9 GRAPHICAL DETERMINATION OF OXIDATION CONSTANTS RCM FACE MATERIAL

Values of A and T_{ox} obtained by estimated best fit lines in Figures 8 and 9 are recorded in Table II. For a check on the validity of these results, the lower portions of the theoretical oxidation parameter curves in Figures 5 and 6 may be referred to. No tests on Matrix II material were made at sufficiently low temperatures to get into the transition regime, so that oxidation constants could not be determined. The values used for the theoretical curves in Figure 4 were based on the values given for commercial graphite in Table II.

Although it is always possible to find a pair of values of AB and T_{ox} by this method, which will fit the test data fairly closely on the oxidation parameter curves, there is insufficient data to determine either one value accurately. Thus, a value for A (or k_o), given independently of T_{ox}, does not define the oxidation performance adequately.

3.4 Determination of Spalling Constants

Experimental values of the oxidation parameter Y obtained in the spalling regime, can be used to determine the spalling constants, once the oxidation constants have been determined. First, we solve for X in Eqn. 2.2.1, using values of A, B, and T_{ox}, as given in Table II. We then re-write Eqn. 2.2.2 in the form

$$P_{SPALL} = (Y - X) h_{EFF} = BC e^{-T_s/T_w} \qquad 3.4.1$$

Taking logarithms of both sides

$$\ln P_{SPALL} = \ln (BC) - T_s/T_w \qquad 3.4.2$$

Thus if experimental values of P_{SPALL} are plotted against $1/T_w$ on semilog paper, the slope of the best fit line is equal to $-T_s \log_{10} e$, and the intercept is equal to $\log_{10} (BC)$. Plots of this type are shown for Matrices II and III respectively in Figures 10 and 11. The values of P_{SPALL} were taken from Table IV.

Values of C and T_s obtained in this way are recorded in Table II, and were used for the theoretical plots of the oxidation parameter in Figures 4 and 5. Insufficient high temperature tests were carried out on the face material to determine its spalling constants, and the theoretical curves in Figure 6 assume the same values as for Matrix II.

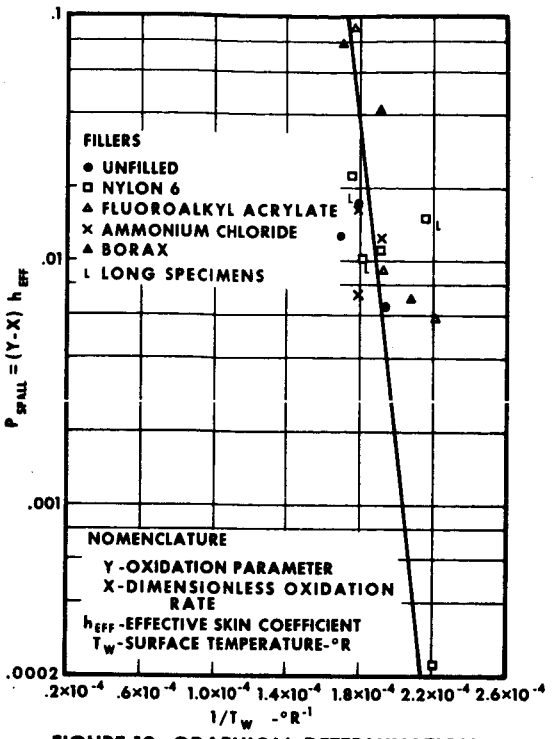

FIGURE 10 GRAPHICAL DETERMINATION OF SPALLING CONSTANTS MATRIX II

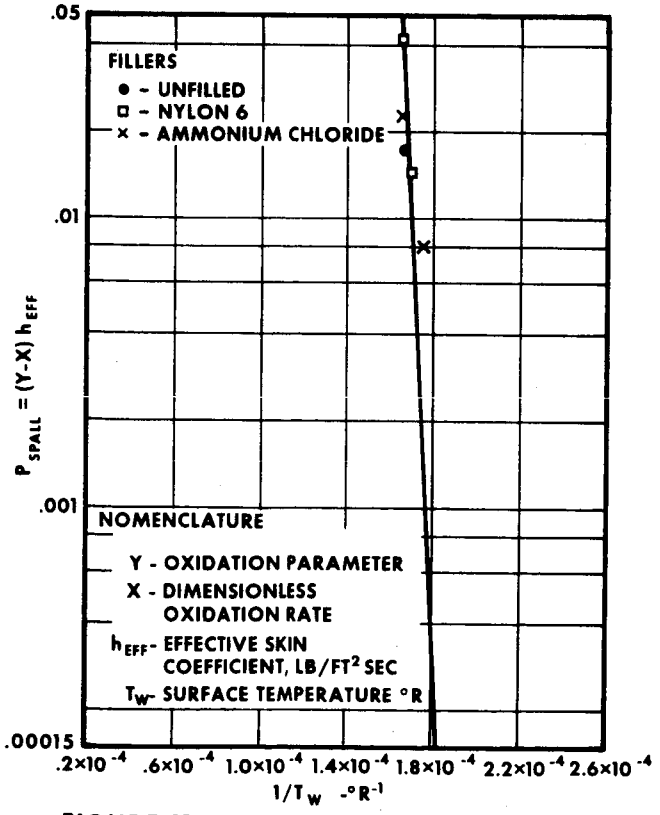

FIGURE 11 GRAPHICAL DETERMINATION OF SPALLING CONSTANTS MATRIX III

REFERENCES

1. Glasstone, et. al., The Theory of Rate Processes, McGraw Hill Book Co., Inc., New York, N. Y., 1st ed., pp. 369-372.

2. Wheeler, A., "Advances in Catalysis," Vol. II, Academic Press Inc., New York, N. Y., 1951, p. 250.

3. Blyholder, George and Eyring, Henry, "Kinetics of Graphite Oxidation," The Journal of Physical Chemistry, Vol. 61, No. 5, May 1957, p. 682.

4. Blyholder, George and Eyring, Henry, "Kinetics of Graphite Oxidation II," The Journal of Physical Chemistry, Vol. 63, No. 6, June 1959, p. 1004.

5. Tu, C. M., et. al., "Combustion Rate of Carbon; Combustion of Spheres in Flowing Gas Stream," Industrial Engineering Chemistry, Vol. 26, July 1934, pp. 749-757.

6. Moore and Zlotnick, "Combustion of Carbon in an Air Stream," ARS Journal, Vol. 31, No. 10, October 1961, pp. 1388-1397.

7. Bradshaw, W., "Oxidation of Graphite and Various Types of Carbon", (preprint, to be presented at Sixth Biennial Conference on Carbon, The University of Pittsburgh, June 17-21, 1963).

8. Hartnett and Eckert, "Mass Transfer Cooling with Combustion in a Laminar Boundary Layer," Heat Transfer and Fluid Mechanics Institute, June 1958, pp. 54-68.

9. Scala, S. M., "Surface Combustion in Dissociated Air," Jet Propulsion, Vol. 28, No. 5, May 1958, pp. 340-341.

10. Cohen, et. al., "Boundary Layers with Chemical Reaction Due to Mass Addition," Jet Propulsion, Vol. 28, No. 10, October, 1958, pp. 659-668.

11. Bromberg and Lipkis, "Heat Transfer in Boundary Layers with Chemical Reactions Due to Mass Addition," Jet Propulsion, Vol. 28, No. 10, October 1958, pp. 668-674.

12. Denison and Dooley, "Combustion in the Laminar Boundary Layer of Chemically Active Sublimating Surfaces," Journal of the Aeronautical Sciences, April 1958, pp. 271-272.

13. R. K. Carlson, et. al., "Carbonized Plastic Composites for Hyperthermal Environments," ASD-TDR-62-352, June 1962.

14. E. J. Nolan and S. M. Scala, "Aerothermodynamic Behavior of Pyrolytic Graphite During Sustained Hypersonic Flight," ARS Journal, Vol. 32, No. 1, January 1962.

15. F. C. Smith, et. al., "Development of a Reinforced Carbonaceous and Ablative Composite for Entry Heat Protection of Manned Spacecraft," Six Month's Progress Report, Vought Astronautics Report No. 330.14, 31 December 1962 (Contract NAS 9-576).

16. F. C. Smith, et. al., "Development of a Reinforced Carbonaceous and Ablative Composite for Entry Heat Protection of a Manned Spacecraft," Quarterly Progress Report, Vought Astronautics Report No. 330.15, 31 March 1963 (Contract NAS 9-576).

17. Hirschfelder, et. al., Molecular Theory of Gases and Liquids, Wiley, New York, 1954.

18. S. M. Scala and E. J. Nolan, "Aerothermodynamic Feasibility of Graphite for Hypersonic Glide Vehicles, Re-Entry and Vehicle Design," Vol. 4, Proc. of the 5th Symposium on Ballistic Missile and Space Technology, Academic Press, New York, 1960, p. 31.

19. W. S. Horton, "Oxidation Kinetics of Pyrolytic Graphite," General Electric Co., G. E. L. Document No. 60 GL 218, January 1961.

APPENDIX

Definition of Terms in Plasma Test Data Summary

Type: Stagn. or Side for stagnation point or side heating test, respectively.

Specimen No: Number used to denote specimen in test series. The Matrix II specimens with capital letter, e.g., II-A-1, are long specimens.

Material: Designation of carbonaceous material and filler as defined in Table I.

A Area of specimen (ft^2).

R_{ox} Ratio of oxygen to carbonaceous material (= 1.33 R_c , where R_c is proportion of carbon, as given in Table see Eqns. 2.1.7, 8 and 9).

ΔM_M Total mass loss of carbonaceous material (lb). By direct measurement on stagnation point specimens. Computed from local recession on side heating specimens. Mass losses computed from recession on the stagnation point face specimens are shown in brackets.

ΔM_A **Total** mass loss of ablative filler (lb). Specimens were run until back face temperature indicated loss of filler.

t Duration of heat pulse in plasma arc test (secs).

c_{ox_e} Mass fraction of oxygen in plasma stream.

B Diffusion parameter; = $R_{ox} / c_{ox_e} (L_{EFF})_{INIT}$

i_R Enthalpy of plasma stream (BTU/lb).

p Local **static** pressure (atmospheres). Stagnation pressure behind shock assumed for stagnation point specimens. Free stream pressure assumed for side heating specimens.

q_{COLD} Cold wall heating rate to calorimeter mounted at stagnation point for stagnation point specimens. Mounted on side of sting for side heating specimens. Reading taken immediately before and after each test run (BTU/ft^2-sec).

T_W Stabilized surface temperature of specimen (°R). Taken by optical pyrometer, and corrected for emissivity and viewing window.

$\dot{M}_{TOT}$ Mass loss rate of carbonaceous material (lb/ft^2-sec).

$= \Delta M_M / tA$

$\dot{M}_A$ Mass loss rate of ablative filler (lb/ft^2-sec).
$= \Delta M_A / tA$

i_w Enthalpy of test medium at wall conditions (BTU/lb), i.e., temperature T_w and pressure p.

Δi Driving enthalpy (BTU/lb) $= i_R - i_w$

q_{HOT} Hot wall heat flux (BTU/ft^2-sec) $= q_{COLD}\, \Delta i / (i_R - i_{COLD})$, ($i_{COLD}$ = 210-260 BTU/lb. for stagnation specimens and 130 BTU/lb. for side heating specimens).

$\dot{M}_E'$ Mass loss rate in diffusion regime (lb/ft^2-sec).
$= (q_{HOT}/\Delta i - K\dot{M}_A)/(B + K)$

This is a solution of the eqns.
$B\dot{M}_E / h_{EFF} = 1$
$h_{EFF} = q_{HOT}/\Delta i - K(\dot{M}_E + \dot{M}_A)$

$\dot{M}_E''$ Lesser of $\dot{M}_E'$ and $\dot{M}_{TOT}$ (lb/ft^2-sec). This is the maximum amount of carbonaceous material which can have oxidized on the surface, and in the boundary layer after spalling, and can therefore have contributed to transpiration cooling.

q_{BLOW} Convective heating rate corrected for transpiration cooling (BTU/ft^2-sec).
$= q_{HOT} - K\Delta i (\dot{M}_E'' + \dot{M}_A)$

(K assumed equal to .67 for all cases).

h_{EFF} Effective skin coefficient (lb/ft^2-sec). $= q_{BLOW}/\Delta i$

Y Oxidation parameter $= B\dot{M}_{TOT}/h_{EFF}$

P_{ox} Quantity used in determining oxidation constants (see Eqn. 3.3.1).
$= \frac{Y^2}{1-Y} \cdot \frac{h_{EFF}^2}{p}$

X Dimensionless oxidation rate (see Eqn. 2.2.3).
$= \frac{1}{2} D \left\{ \sqrt{D^2 + 4} - D \right\}$
where $D = \frac{AB p^{1/2} e^{-T_{ox}/T_w}}{h_{EFF}}$

For Matrix II and face material, $X \approx 1$ in the spalling regime. For Matrix III material, A and T_{ox} are taken from Table II.

P_{SPALL} Quantity used in determining spalling constants (see Eqn. 3.4.1).
$= (Y - X) h_{EFF}$

PLASMA TEST DATA SUMMARY

Type	Stagn.	Stagn.	Stagn.	Stagn.	Stagn.	Stagn.
Specimen No.	II-a-1	II-a-2	II-a-3	II-b-1	II-b-2	II-b-3
Material	Matrix II	Matrix II	Matrix II	Matrix II Polystyrene	Matrix II Polystyrene	Matrix II Polystyrene
A	.00304	.00304	.00305	.00304	.00306	.00304
R_{ox}	1.3333	1.3333	1.3333	1.3333	1.3333	1.3333
ΔM_M	.001980	.001630	.000990	.001930	.000510	.000620
ΔM_A	0	0	0	.003200	.003150	.003240
t	115.0	67.0	33.0	142.0	48.5	42.0
c_{ox_e}	.23	.23	.23	.23	.23	.23
B	5.80	5.80	5.80	5.80	5.80	5.80
i_R	5350	9650	14300	5350	9500	14600
P	.05068	.06245	.07007	.05068	.06122	.07075
q_{COLD}	226	418	692	226	398	719
T_w	4520	5140	5880	4510	5050	5700
$\dot{M}_{TOT}$	.005660	.007980	.009830	.004470	.003440	.004860
$\dot{M}_A$	0	0	0	.007410	.021220	.025380
i_w	1400	1880	2750	1400	1800	2550
Δi	3950	7770	11550	3950	7700	12050
q_{HOT}	173	345	569	173	330	603
$\dot{M}_E$	.006770	.006860	.007610	.006000	.004430	.005110
$\dot{M}_E$	.005660	.006860	.007610	.004470	.003440	.004860
q_{SLOW}	158.0	309.3	510.1	141.6	202.8	358.9
h_{EFF}	.040010	.039810	.044200	.035800	.026300	.029800
γ	.8208	1.1628	1.2898	.7243	.7586	.9460
P_{ox}	---	---	---	---	---	---
X	---	1.0	1.0	---	---	---
P_{SPALL}	---	.00648	.01281	---	---	---

PLASMA TEST DATA SUMMARY (Cont'd)

Type	Stagn.	Stagn.	Stagn.	Stagn.	Stagn.	Stagn.
Specimen No.	II-c-1	II-c-2	II-c-3	II-d-1	II-d-2	II-d-3
Material	Matrix II Nylon 6	Matrix II Nylon 6	Matrix II Nylon 6	Matrix II Fluor Acr	Matrix II Fluor Acr	Matrix II Fluor Acr
A	.00304	.00305	.00305	.00305	.00305	.00304
R_{ox}	1.3333	1.3333	1.3333	1.3333	1.3333	1.3333
ΔM_M	.000990	.000970	.001020	.000700	.000830	.002600
ΔM_A	.002980	.002830	.002910	.004060	.004310	.002580
t	64.0	48.5	39.0	48.5	50.0	40.0
c_{ox_e}	.23	.23	.23	.23	.23	.23
B	5.80	5.80	5.80	5.80	5.80	5.80
i_R	5400	9500	14600	5400	9500	14600
ρ	.05102	.06122	.07075	.05102	.06122	.07075
q_{COLD}	224	398	674	221	406	707
T_w	4520	5230	5680	4520	5190	5640
$\dot{M}_{TOT}$	.005090	.006560	.008580	.004730	.005440	.021380
$\dot{M}_A$	.015320	.019130	.024460	.027450	.028260	.021220
i_w	1400	2000	2520	1450	1940	2500
Δi	4000	7500	12080	3950	7560	12100
q_{HOT},	172	322	567	168	332	596
$\dot{M}_E$,	.005060	.004650	.004720	.003730	.003860	.005420
$\dot{M}_E$'	.005060	.004650	.004720	.003730	.003860	.005420
q_{BLOW}	117.4	202.5	330.8	85.5	169.3	380.0
h_{EFF}	.029300	.027000	.027400	.021640	.022400	.031400
Y	1.0075	1.4093	1.8161	1.2676	1.4085	3.9490
P_{ox}	---	---	---	---	---	---
X	1.0	1.0	1.0	1.0	1.0	1.0
P_{SMALL}	.00022	.01105	.02236	.00579	.00915	.09260

PLASMA TEST DATA SUMMARY (Cont'd)

Type	Stagn.	Stagn.	Stagn.	Stagn.	Stagn.	Stagn.
Specimen No.	II-e-1	II-e-2	II-e-3	II-g-1	II-g-2	II-g-3
Material	Matrix II Amm Chl	Matrix II Amm Chl	Matrix II Amm Chl	Matrix II Borax	Matrix II Borax	Matrix II Borax
A	.00304	.00304	.00305	.00305	.00305	.00305
R_{ox}	1.3333	1.3333	1.3333	1.3333	1.3333	1.3333
ΔM_M	.000900	.000940	.001410	.003420	.003300	.004940
ΔM_A	.001510	.001450	.001440	.003240	.003500	.002910
t	63.0	40.0	50.0	168.0	98.0	94.0
c_{ox_e}	.23	.23	.23	.23	.23	.23
B	5.80	5.80	5.80	5.80	5.80	5.80
i_R	5500	9500	14500	5600	9750	14500
P	.05136	.06122	.07041	.05170	.06218	.07080
q_{COLD}	230	412	684	214	316	458
T_w	4610	5220	5560	4810	5240	5840
$\dot{M}_{TOT}$	.004700	.007730	.009250	.006670	.011040	.017230
$\dot{M}_A$	.007880	.011920	.009440	.006320	.011710	.010150
i_w	1450	1960	2400	1600	2000	2700
Δi	4050	7540	12100	4000	7750	11800
q_{HOT}	176	335	580	158	258	380
$\dot{M}_E$,	.005900	.005790	.006430	.005450	.005650	.006360
$\dot{M}_E$'	.004700	.005790	.006430	.005450	.005650	.006360
q_{SLOW}	141.9	245.5	451.3	126.5	167.9	249.5
h_{EFF}	.035000	.032600	.037300	.031600	.021700	.021100
Y	.7789	1.3752	1.4383	1.2244	2.9507	4.7360
P_{ox}	---	---	---	---	---	---
X	---	1.0	1.0	1.0	1.0	1.0
P_{SPALL}	---	.01223	.01635	.00709	.04233	.07883

PLASMA TEST DATA SUMMARY (Cont'd)

Type	Stagn.	Stagn.	Stagn.	Stagn.	Stagn.	Stagn.
Specimen No.	II-A-1	II-A-2	II-A-3	II-C-1	II-C-2	II-C-3
Material	Matrix II	Matrix II	Matrix II	Matrix II Nylon 6	Matrix II Nylon 6	Matrix II Nylon 6
A	.00308	.00307	.00306	.00307	.00307	.00307
R_{ox}	1.3333	1.3333	1.3333	1.3333	1.3333	1.3333
ΔM_M	.001300	.001520	.002200	.001910	.002170	.001910
ΔM_A	0	0	0	.005380	.004940	.005400
t	244.0	61.0	69.0	135.0	95.0	90.0
c_{ox_e}	.23	.23	.23	.23	.23	.23
B	5.80	5.80	5.80	5.80	5.80	5.80
i_R	5400	9300	14400	5400	9300	14300
ρ	.05068	.06122	.07075	.05068	.06109	.07007
q_{COLD}	242	482	682	239	502	730
T_w	4260	5060	5540	4340	4960	5510
$\dot{M}_{TOT}$	.005770	.008120	.010400	.004600	.007430	.006930
$\dot{M}_A$	0	0	0	.012980	.016900	.019600
i_w	1260	1800	2350	1280	1960	2320
Δi	4140	7500	12050	4120	7540	11980
q_{HOT},	194	398	580	189	335	622
$\dot{M}_E$,	.007240	.008200	.007440	.005740	.005120	.006000
$\dot{M}_E$	.005770	.008120	.007440	.004600	.005120	.006000
q_{BLOW}	178.0	358.8	519.9	143.2	210.8	361.5
h_{EFF}	.043000	.047800	.043100	.034800	.028100	.029930
Y	.7784	.9854	1.3995	.7667	1.5335	1.3428
P_{ox}	---	---	---	---	---	---
X	---	---	1.0	---	1.0	1.0
P_{SPALL}	---	---	.01722	---	.01499	.01026

PLASMA TEST DATA SUMMARY (Cont'd)

Type	Stagn.	Stagn.	Stagn.	Stagn.	Stagn.	Stagn.
Specimen No.	II-B-1	II-B-2	II-B-3	III-a-1	III-a-2	III-a-3
Material	Matrix II Amm Chl	Matrix II Amm Chl	Matrix II Amm Chl	Matrix III	Matrix III	Matrix III
A	.00308	.00308	.00308	.00296	.00296	.00296
R_{ox}	1.3333	1.3333	1.3333	1.2226	1.1560	1.2000
ΔM_M	.001770	.001770	.002360	.000060	.000140	.000430
ΔM_A	.002860	.002500	.002920	0	0	0
t	131.0	82.0	94.0	22.7	13.0	16.0
c_{ox_e}	.23	.23	.23	.23	.23	.23
B	5.80	5.80	5.80	5.32	5.03	5.22
i_R	5400	9300	14300	3500	8000	13000
ρ	.05068	.06122	.07007	.05170	.06333	.07177
q_{COLD}	242	500	724	144	326	590
T_w	4490	5130	5590	4420	5340	5960
$\dot{M}_{TOT}$	.004390	.007010	.008150	.000950	.003540	.009000
$\dot{M}_A$	.007090	.009900	.010090	0	0	0
i_w	1380	1870	2420	1330	2100	2850
Δi	4020	7430	11880	2170	5900	10150
q_{HOT},	187	409	612	94	248	470
$\dot{M}_E$,	.006460	.007480	.006920	.007230	.007370	.007860
$\dot{M}_E$'	.004390	.007010	.006920	.000950	.003540	.007860
q_{BLOW}	157.9	324.8	476.6	92.6	234.0	446.6
h_{EFF}	.039280	.043720	.040120	.042680	.039660	.041040
γ	.6482	.9300	1.1782	.1291	.4491	1.1447
P_{ox}	---	---	---	.000597	.006275	---
X	---	---	1.0	.15276	.49843	.72578
P_{SMALL}	---	---	.00715	---	---	.01719

PLASMA TEST DATA SUMMARY (Cont'd)

Type	Stagn.	Stagn.	Stagn.	Stagn.	Stagn.	Stagn.
Specimen No.	III-c-1	III-c-2	III-c-3	III-e-1	III-e-2	III-e-3
Material	Matrix III Nylon 6	Matrix III Nylon 6	Matrix III Nylon 6	Matrix III Amm Chl	Matrix III Amm Chl	Matrix III Amm Chl
A	.00296	.00296	.00296	.00290	.00289	.00290
R_{ox}	1.2000	1.2266	1.2320	1.1933	1.1813	1.1813
ΔM_M	.000790	.000670	.001150	0	.000420	.000690
ΔM_A	.003040	.003500	.003450	.001140	.001640	.001040
t	66.1	42.5	33.6	39.0	29.0	25.3
c_{ox_e}	.23	.23	.23	.23	.23	.23
B	5.22	5.33	5.36	5.19	5.14	5.14
i_R	3500	10350	13000	3500	9800	13000
ρ	.05136	.06293	.07143	.05116	.06190	.07143
q_{COLD}	138	365	572	129	374	563
T_w	4420	5860	6040	3680	5720	6020
$\dot{M}_{TOT}$	.004040	.005330	.011520	0	.005010	.009400
$\dot{M}_A$	.015540	.027820	.034570	.010080	.019570	.014170
i_w	1330	2730	2920	1000	2600	2900
Δi	2170	7620	10080	2500	7200	10100
q_{HOT}	91	275	452	97	282	446
$\dot{M}_E$'	.005350	.002910	.003600	.005470	.004490	.005970
$\dot{M}_E$''	.004040	.002910	.003600	0	.004490	.005970
q_{SLOW}	62.5	118.1	194.2	80.1	155.9	309.7
h_{EFF}	.028820	.015500	.019270	.032050	.021660	.030660
Y	.7318 ?	1.8329	3.1028	0	1.1888	1.5760
P_{ox}	.018650 ?	---	---	---	---	---
X	.21800 ?	.91149	.91541	---	.81736	.82103
P_{SMALL}	.01480 ?	.01428	.04215	---	.00805	.02315

PLASMA TEST DATA SUMMARY (Cont'd)

Type	Stagn.	Stagn.	Stagn.	Stagn.	Stagn.	Stagn.
Specimen No.	P1	P2	P3	P4	P5	P6
Material	Face	Face	Face	Face	Face	Face
A	.00304	.00305	.00305	.00304	.00301	.00304
R_{ox}	1.3333	1.3333	1.3333	1.3333	1.3333	1.3333
ΔM_M	.001060 [.001030]	.000980 [.000830]	.000390 [.000860]	.000940 [.000950]	.001180 [.001190]	.001040 [.001080]
ΔM_A	0	0	0	0	0	0
t	69.5	75.0	73.0	70.0	70.0	54.5
c_{ox_e}	.23	.23	.23	.23	.23	.23
B	5.80	5.80	5.80	5.80	5.80	5.80
i_R	10800	6700	6850	9000	15900	16633
ρ	.02640	.02300	.02320	.02510	.02740	.02820
q_{COLD}	348	202	210	280	395	480
T_w	4938	4195	4539	4488	4990	5224
$\dot{M}_{TOT}$	.005017	.004109	.004176	.004417	.005600	.006277
$\dot{M}_A$	0	0	0	0	0	0
i_w	1830	1250	1440	1570	1870	1760
Δi	8970	5450	5810	7430	14030	14873
q_{HOT},	296	170	172	237	354	436
$\dot{M}_E$,	.005103	.004833	.004910	.004940	.003903	.004531
$\dot{M}_E$'	.005017	.004109	.004176	.004417	.003903	.004531
q_{SLOW}	266.0	155.4	156.7	215.5	317.6	390.9
h_{EFF}	.029656	.028517	.028970	.022904	.022640	.026281
γ	.9812	.8357	.3361	.8833	1.4346	1.3853
P_{ox}	---	---	---	---	---	---
X	---	---	---	---	---	---
P_{SPALL}	---	---	---	---	---	---

PLASMA TEST DATA SUMMARY (Cont'd)

Type	Stagn.	Stagn.	Stagn.	Stagn.	Stagn.	Stagn.
Specimen No.	P_7	P_8	P_9	P_{10}	P_{11}	P_{12}
Material	Face	Face	Face	Face	Face	Face
A	.00304	.00302	.00304	.00304	.00305	.00304
R_{ox}	1.3333	1.3333	1.3333	1.3333	1.3333	1.3333
ΔM_M	.000580 [.000670]	.000240 [.000160]	.000430 [.000460]	.000370 [.000250]	.000970 [.000980]	.001060 [.000860]
ΔM_A	0	0	0	0	0	0
t	138.3	161.0	93.0	283.0	55.5	280.6
c_{ox_e}	0	0	0	0	.23	.05
B	∞	∞	∞	∞	5.80	26.67
i_R	8708	3590	10175	3391	15108	6358
ρ	.02260	.01650	.02320	.01590	.02760	.01930
q_{COLD}	439	155	460	139	433	206
T_w	3664	3312	4958	3569	5190	4194
$\dot{M}_{TOT}$	.001379	.000493	.001520	.000430	.005730	.001242
$\dot{M}_A$	0	0	0	0	0	0
i_w	1000	880	1860	960	2140	1250
Δi	7608	2710	8315	2431	12968	4118
q_{HOT}	400	124	386	105	378	139
$\dot{M}_B$	0	0	0	0	.004507	.001232
$\dot{M}_E$	0	0	0	0	.004507	.001232
q_{BLOW}	---	---	---	---	339.0	135.3
h_{EFF}	---	---	---	---	.026143	.033234
γ	---	---	---	---	1.2712	1.0085
P_{ox}	---	---	---	---	---	---
X	---	---	---	---	---	---
P_{SHALL}	---	---	---	---	---	---

PLASMA TEST DATA SUMMARY (Cont'd)

Type	Stagn.	Stagn.	Stagn.	Stagn.	Stagn.
Specimen No.	P_{13}	P_{14}	P_{15}	P_{16}	P_{17}
Material	Face	Face	Face	Face	Face
A	.00305	.00305	.00304	.00304	.00304
R_{ox}	1.3333	1.3333	1.3333	1.3333	1.3333
ΔM_M	.000250 [.000210]	.001430 [.001280]	.000900 [.000940]	.000970 [.000830]	.001560 [.001600]
ΔM_A	0	0	0	0	0
t	36.0	141.0	184.0	145.0	104.0
c_{ox_e}	.10	.10	.0	.10	.23
B	13.33	13.33	∞	13.33	5.80
i_R	6100	12817	11258	6517	12270
ρ	.02140	.02570	.02080	.02170	.02640
q_{COLD}	211	483	538	223	402
T_w	4100	5182	5398	4380	4920
$\dot{M}_{TOT}$	.002276	.003325	.001608	.002200	.004934
$\dot{M}_A$	0	0	0	0	0
i_w	1200	2140	2470	1360	1880
Δi	4900	10677	8788	5157	10390
q_{HOT}	176	407	430	183	348
$\dot{M}_E$,	.002572	.002722	0	.002538	.005173
$\dot{M}_E$*	.002276	.002722	0	.002200	.004934
q_{BLOW}	169.0	387.3	---	165.6	313.4
h_{EFF}	.034482	.036276	---	.032114	.030166
Y	.8799	1.2218	---	.9132	.9487
P_{ox}	---	---	---	---	---
X	---	---	---	---	---
P_{SPALL}	---	---	---	---	---

PLASMA TEST DATA SUMMARY (Cont'd)

Type	Side	Side	Side	Side	Side	Side
Specimen No.	SH-1	SH-2	SH-4	SH-5	SH-6	SH-7
Material	Face	Face	Face	Face	Face	Face
A	.00640	.00640	.00642	.00656	.00656	.00665
R_{ox}	1.3333	1.3333	1.3333	1.3333	1.3333	1.3333
ΔM_M	.000036	.000359	.000093	.000500	.000457	.000024
ΔM_A	0	0	0	0	0	0
t	121.0	120.0	121.0	120.0	119.5	488.0
c_{ox_e}	.23	.23	.23	.23	.23	0
B	5.80	5.80	5.80	5.80	5.80	∞
i_R	5130	10600	5500	13500	13450	4724
ρ	.00156	.00293	.00177	.00333	.00333	.00068
q_{COLD}	8.50	32.70	10.65	49.00	53.50	9.18
T_w	2223	2822	2218	3263	3270	2040
$\dot{M}_{TOT}$	.000047	.000467	.000119	.000635	.000583	.000007
$\dot{M}_A$	0	0	0	0	0	0
i_w	570	740	570	870	880	520
Δi	4560	9860	4930	12630	12570	4204
q_{HOT},	7.77	30.82	9.80	46.32	50.50	8.43
$\dot{M}_E$,	.000263	.000483	.000307	.000567	.000621	0
$\dot{M}_E$*	.000047	.000467	.000119	.000567	.000583	0
q_{BLOW}	7.63	27.99	9.44	41.52	45.62	---
h_{EFF}	.001673	.002839	.001915	.003287	.003629	---
Y	.1632	.9542	.3603	1.1205	.9317	---
P_{ox}	.000057 ?	.054690	.000421	---	---	---
X	---	---	---	---	---	---
P_{SPALL}	---	---	---	---	---	---

PLASMA TEST DATA SUMMARY (Cont'd)

Type	Side	Side	Side	Side	Side	Side
Specimen No.	SH-8	SH-9	SH-10	SH-11	SH-12	SH-13
Material	Face	Face	Face	Face	Face	Face
A	.00657	.00660	.00653	.00663	.00662	.00661
R_{ox}	1.3333	1.3333	1.3333	1.3333	1.3333	1.3333
ΔM_M	.000070	.000075	.000362	0	.000655	.000218
ΔM_A	0	0	0	0	0	0
t	480.0	428.0	75.0	71.0	150.0	70.0
c_{ox_e}	.0	0	.23	.23	.23	.23
B	∞	∞	5.80	5.80	5.80	5.80
i_R	10835	17095	14300	6650	12800	10000
P	.00153	.00255	.00306	.00119	.00255	.00323
q_{COLD}	30.30	51.80	68.04	11.80	58.32	41.00
T_w	2606	2974	3436	2220	3234	2926
$\dot{M}_{TOT}$	.000022	.000026	.000739	0	.000660	.000471
$\dot{M}_A$	0	0	0	0	0	0
i_w	670	780	950	560	860	770
Δi	10165	16315	13350	6090	11940	9230
q_{HOT},	28.80	49.84	64.15	11.04	55.00	38.38
$\dot{M}_E$,	0	0	.000743	---	.001712	.0006343
$\dot{M}_E$'	0	0	.000739	---	.000660	.000471
q_{BLOW}	---	---	57.54	---	49.72	35.47
h^o_{EFF}	---	---	.004310	---	.004164	.0038843
Y	---	---	.9944	---	.9193	.7106
P_{ox}	---	---	---	---	---	---
X	---	---	---	---	---	---
P_{SPALL}	---	---	---	---	---	---

PLASMA TEST DATA SUMMARY (Cont'd)

Type	Side	Side	Side	Side	Side	Side
Specimen No.	SH-14	SH-15	SH-16	SH-17	SH-18	SH-19
Material	Face	Face	Face	Face	Face	Face
A	.00654	.00653	.00659	.00656	.00660	.00656
R_{ox}	1.3333	1.3333	1.3333	1.3333	1.3333	1.3333
ΔM_M	.000435	.000199	0	.000097	.000617	.000650
ΔM_A	0	0	0	0	0	0
t	99.5	961.0	468.0	480.0	960.0	480.0
c_{oxe}	.23	0	0	0	.05	.10
B	5.80	∞	∞	∞	26.67	13.33
i_R	11100	8331	7110	10691	9758	7608
ρ	.00323	.00153	.00153	.00255	.00170	.00204
q_{COLD}	55.60	41.44	17.00	57.10	28.48	28.51
T_w	3061	2717	2165	2744	2690	2750
$\dot{M}_{TOT}$	.000662	.0000032	0	.000031	.000097	.000206
$\dot{M}_A$	0	0	0	0	0	0
i_w	820	720	550	720	700	720
Δi	10280	7611	6560	9971	9058	6888
q_{HOT}	52.15	38.51	16.00	53.96	26.82	26.30
$\dot{M}_E'$	.000784	0	0	0	.000108	.000273
$\dot{M}_E^*$	.000662	0	0	0	.000097	.000206
q_{BLOW}	47.59	---	---	---	26.23	25.35
h_{EFF}	.004629	---	---	---	.002896	.003680
Y	.8296	---	---	---	.8933	.7462
P_{ox}	---	---	---	---	.036900	.014390
X	---	---	---	---	---	---
P_{SPALL}	---	---	---	---	---	---

PLASMA TEST DATA SUMMARY (Cont'd)

Type	Side	Side	Side	Side	Side	Side
Specimen No.	SH-20	Spare 2	Spare 3	SH-1R	SH-2R	SH-10R
Material	Face	Face	Face	Face	Face	Face
A	.00656	.00657	.00667	.00650	.00618	.00626
R_{ox}	1.3333	1.3333	1.3333	1.3333	1.3333	1.3333
ΔM_M	.000095	.001470	.002350	.000194	.000902	.000931
ΔM_A	0	0	0	0	0	0
t	242	235	240	240	240	240
C_{ox_e}	.23	.23	.23	.23	.23	.23
B	5.80	5.80	5.80	5.80	5.80	5.80
i_R	3850	12400	10600	5400	11000	13000
P	.00102	.00255	.00323	.00156	.00279	.00340
q_{COLD}	9.67	60.75	57.78	8.30	33.30	59.40
T_w	2085	3177	3277	2195	2832	3116
$\dot{M}_{TOT}$	.000060	.000938	.000845	.000124	.000608	.000619
$\dot{M}_A$	0	0	0	0	0	0
i_w	540	850	880	560	740	830
Δi	3310	11550	9720	4840	10260	12170
q_{HOT}	8.63	57.23	53.69	7.62	31.90	56.17
$\dot{M}_E$	.000403	.000766	.000854	.000243	.000481	.000713
$\dot{M}_E$	.000060	.000766	.000854	.000124	.000481	.000619
q_{BLOW}	8.50	51.30	48.19	7.22	28.60	51.12
h_{EFF}	.002570	.004442	.004958	.001491	.002788	.004200
Y	.1353	1.2247	.9885	.4822	1.2647	.8548
P_{ox}	.000137	---	---	.063990	---	---
X	---	---	---	---	---	---
P_{SMALL}	---	---	---	---	---	---

PLASMA TEST DATA SUMMARY (Cont'd)

Type	Side	Side	Side	Side
Specimen No.	SH-11R	SH-13R	SH-14R	SH-20R
Material	Face	Face	Face	Face
A	.00668	.00644	.00633	.00649
R_{ox}	1.3333	1.3333	1.3333	1.3333
ΔM_M	.000296	.001092	.000962	.000131
ΔM_A	0	0	0	0
t	240	240	240	240
c_{oxe}	.23	.23	.23	.23
B	5.80	5.80	5.80	5.80
i_R	5800	10000	12000	5600
p	.00224	.00361	.00374	.00157
q_{COLD}	12.15	37.50	52.11	9.72
T_w	2319	3067	3011	2041
$\dot{M}_{TOT}$	.000184	.000706	.000633	.000084
$\dot{M}_A$	0	0	0	0
i_w	600	820	790	550
Δi	5050	11210	9180	5200
q_{HOT},	11.14	34.88	49.21	9.08
$\dot{M}_E$,	.000331	.000587	.000679	.000273
$\dot{M}_E$*	.000184	.000587	.000633	.000084
q_{SLOW}	10.50	31.27	44.46	8.80
h_{EFF}	.002019	.003406	.003966	.001743
Y	.5285	1.2023	.9256	.2794
P_{ox}	.001078	---	.048430	.000211
X	---	---	---	---
P_{SMALL}	---	---	---	---